An Innovative Organic Rankine Cycle Approach for High Temperature Applications

Angad Singh Panesar
School of Computing, Engineering and Mathematics, University of Brighton

Abstract

Organic Rankine Cycles (ORC) using toluene and hexamethyldisiloxane (MM) are put forward as a means of improving the efficiency of automotive heavy duty engines, and provide a reference for comparison in this study. Despite an efficiency improvement potential of 4-4.7%, the current ORC approach is not reaching the required fuel savings within the expected costs. As such, innovative pathways to improve the ORC performance and cost-effectiveness are of great importance to the research community. This paper presents a partial solution by means of a conceptual overview and simulation results for ORCs especially tailored for high-temperature applications. A fundamental revision of the heat transfer and expansion characteristics is presented, without increasing the system integration complexity. These characteristics are attributed to the use of formulated organic blends with toluene and MM as a significant blend component. The developed 22 criteria blend screening methodology is presented. Simulation results show that for an equivalent expansion volume flow ratio, and product of heat transfer coefficient and area, the blends offer a 22-24% improvement in the net power. This resulted in a 15-18% cost savings compared to the reference ORC. The simulations were conducted in Aspen HYSYS V8 using the Peng-Robinson and Wilson fluid property packages.

Keywords

Organic Rankine cycles; Internal combustion engines; Size and performance trade-off; Irreversibilities; High-temperature organic blends; Cost analysis

Nomenclature

A	heat transfer area (m^2)
c_p	specific heat (kJ/kg°C)
D	diameter (m)
h	specific enthalpy (kJ/kg)
H_{vap}	latent heat of vaporisation (kJ/kg)
$\dot{I}$	irreversibility (kW)
L	volume (L)

E-mail address: A.Panesar@brighton.ac.uk
Tel: +44 (0)1273 642313

$\dot{m}$	mass flow rate (kg/s)
M_{wt}	molecular weight (g/mol)
P	absolute pressure (bar)
$\dot{Q}$	thermal duty (kW)
S	turbine size parameter (m)
s	specific entropy (kJ/kg°C)
T	temperature (°C)
U	overall heat transfer coefficient (W/m^2°C)
$\dot{V}$	volume flow rate (m^3/s)
$\dot{W}$	power (kW)

Greek symbols

η	efficiency
ρ	density (kg/m^3)
λ	thermal conductivity (W/m°C)
μ	viscosity (cP)

Abbreviations

B100	mid-speed high-load
BTE	brake thermal efficiency
GWP	global warming potential
HDDE	heavy duty diesel engine
HEX	heat exchanger
ICE	internal combustion engine
IHE	internal heat exchanger
MM	hexamethyldisiloxane
MM80	organic blend containing 80 % hexamethyldisiloxane by mass
ORC	organic Rankine cycle
PRV	pressure reducing valve
T80	organic blend containing 80 % toluene by mass
VFR	volume flow ratio
VLE	vapour-liquid equilibrium

Subscripts

amb	ambient

cond	condenser
exh	exhaust
exp	expander
pp	pinch point

1 Introduction

The modern automotive Internal Combustion Engine (ICE) rejects up to 50% of the total fuel chemical energy in the form of waste heat, with a significant portion of this as high quality exhaust gases. Due to increasing greenhouse emissions and impending worldwide fuel consumption regulations, there is a growing interest in technologies that can even partially utilise the exhaust heat to improve the overall Brake Thermal Efficiency (BTE). This has been an intensified area of research in the last decade, where numerous methods including turbocompounding, thermoelectric generators and fluid bottoming cycles have been proposed and demonstrated for on-road vehicles [1, 2]. The potential fuel consumption reduction using any heat-to-power conversion technology is firstly dependent at least on the ICE application and the duty cycle. Highest benefits are expected in long-haul trucking which involves extended time of running at near steady speeds. As a result, it has been shown that such technologies can play a significant part in achieving future BTE goals for Heavy Duty Diesel Engines (HDDE) [3, 4]. With a focus on automotive exhaust applications, the following overview is divided into four themes: the preferred fluid bottoming cycle, optimisation of ORCs, selection of working fluids, component developments, and integration with other energy technologies and heat sources.

Amongst the fluid bottoming cycle options, Rankine, Kalina and Organic Rankine Cycles (ORC) are typically proposed. The conventional Rankine cycle presents an environmentally friendly and thermally stable solution. However, it offers challenges relating to freezing temperatures, reduced performance under cooler exhaust temperatures, requirement of higher superheating levels, relatively poor transient response and poor turbine efficiency for low capacity applications [5, 6]. The Kalina cycle, which has been initially applied to geothermal applications, offers the advantage of a good temperature match in the heat exchanger using an ammonia-water mixture. Additionally, variation in the composition of the mixture allows adapting the cycle to possible fluctuating heat source and/or sink temperatures. However, it presents challenges relating to packaging of the separator and the Internal Heat Exchanger (IHE), complexity in exploiting different heat streams simultaneously, higher system pressures, and corrosion and stress cracking with some common engineering materials [7, 8]. The frequently cited above reasons hinder the adoption of Rankine and Kalina cycles for automotive applications. As a result, the literature review indicated that the use of relatively simple ORC systems appears to be the leading heat-to-power conversion technology for long-haul truck applications when considering, quality of heat sources (< 450 °C), output capacities (5-25 kW), conversion

efficiencies (10-15%), transient driving conditions, technology readiness level, absolute fuel consumption, space availability and weight penalty [9, 10].

The overall conversion efficiency of an ORC largely depends on the selected working fluid (e.g. refrigerant, hydrocarbon), its associated cycle operating mode (e.g. subcritical, supercritical), the chosen expansion machine (e.g. piston expander, radial turbine) and the system architecture (e.g. thermal, sub-system) [9, 11]. This presents a complex multi-dimensional challenge to find universal solutions, which are vital to reach the economies-of-scale. Attempts using, regression models for evaluating design implications, parametric and thermo-economic optimisation using genetic algorithms and energy integration methodologies coupled with multi-objective optimisation, have all been considered in the literature [12-15]. Adding to the above challenge, organic fluids present the drawbacks of thermal stabilities much below the exhaust gas temperatures, and/or environmental and safety concerns.

For low-temperature exhaust heat, Domingues et al. suggested the use of R245fa due to the higher heat exchanger effectiveness over water [5]. Whereas, for medium-temperature exhaust heat, Larsen et al. showed ethanol as a suitable option [11]. With an increased emphasis on Global Warming Potential (GWP), Yang et al. recently indicated an ultra-low GWP refrigerant (R1234yf) optimal from a thermo-economic point of view [16]. To offer improved thermal stability options, Fernandez et al. recommended hexamethyldisiloxane (MM), while Seher et al. showed a higher performance potential using toluene [17, 18]. Additionally, the modelling study to provide optimisation guidelines by Maraver et al. also suggested the use of toluene [19].

Key ORC components such as heat exchangers and expanders are additionally becoming more viable due to a series of recent technological advancements and similarity to the current automotive components. Yang et al. and Zhang et al. have recently demonstrated prototypes of fin-tube and spiral-tube evaporators, respectively [12, 20]. Zhang et al. have additionally achieved adiabatic efficiencies in excess of 70% with a single-screw expander [20]. While, Wang et al. demonstrated a nominal 5kW heat activated cooling unit under laboratory conditions and achieved isentropic efficiencies in excess of 80% with a scroll expander [21].

ORCs have also been proposed in combination with other technologies including refrigeration cycles and thermoelectric generators. Simulation results by Yılmaz et al. showed that the air-conditioning needs of an intercity bus can be realised using the exhaust gas energy in combination with R134a and R245fa as the working fluids [22]. While, Shu et al. considered the use of thermoelectric generators for higher temperature heat recovery, followed by ORCs for lower temperature heat recovery in a theoretical study [23]. This architecture was suggested primarily to address the thermal stability issue of organic fluids. To exploit exhaust gas and engine coolant heat simultaneously,

dual-loop cascade arrangements and thermal-oil loop transferring the coolant and exhaust heat were also theoretically considered [24, 25]. These configurations allowed higher heat exploitation, however, the challenges relating to system size, weight, cost, control and complexity could be prohibitive for automotive applications.

It is important to highlight that the above reviewed simulation and experimental studies were found to produce a broad range of overall BTE increase (1-6% in absolute terms) for the considered base engines. This was because different studies have utilised different engine platforms, engine speed-load points, heat sources, qualities, quantities, working fluids, ORC system architecture, boundary conditions and component efficiencies, giving different overall conversion efficiencies. Furthermore, the rebound effect was acknowledged in very few of the reviewed studies, i.e. fuel improvements may encourage the consumption of other energy forms which may partially offset the gains [3, 26]. Since the interpretation of the published results is not straight forward, it is advantageous to re-simulate a reference case for comparison.

This paper firstly presents the simulation results for two higher thermal stability conventional ORCs using an IHE to act as a reference for comparison. The reference results were the end product of a system size and system performance trade-off study to quantify the practical improvement potential. Secondly, the shortcomings of such conventional ORCs targeting automotive exhaust heat recovery are detailed. Thirdly, to partially address the shortcomings and facilitate the introduction of ORC systems, an innovative ORC approach is presented conceptually. To realise the proposed ORC approach, fluid blends with unique heat transfer and expansion characteristics are formulated, extending the analysis of parallel works [9, 27]. For equivalent heat transfer footprint and the expansion machine size, the performance variation between the reference ORC and the proposed ORC is calculated. Finally, the economic analysis based on the estimates from step count and exponential methods is presented to quantify the benefit of the proposed ORC approach. For a comprehensive understanding, the system and performance parameters were based on the energy and exergy equations in all the specific points of the cycle. The advanced modelling tool, Aspen HYSYS V8 was used, which contains physical, chemical and thermodynamic data for a wide variety of chemical compounds, as well as a selection of thermodynamic models required for accurate simulation of thermal and chemical systems [28].

2 Reference ORC

2.1 System overview

The ICE offers at least four streams of waste heat, namely, exhaust gases, engine coolant, engine lubricant and charge air. However, only exhaust heat recovery, downstream of the aftertreatment devices, from a 12.8 litre (L), Euro 6, truck engine model was considered at the mid-speed high-load condition (B100) [29]. This was so, since

performance and economic competitiveness of typical fluid bottoming cycles is proportional to the energy and exergy levels of the targeted heat source, respectively. Targeting exhaust heat then provides a good starting point and an attractive opportunity for reducing emissions whilst using a wasted resource. Furthermore, it is important to bear in mind that the present market niche for automotive ORCs is dependent on architectural simplicity. Hence, ORCs with turbine-bleeding arrangements that have shown thermodynamic and economic merits in other applications are not considered practical here [30]. Table 1 summarises some of the engine performance parameters at B100, the input variables for heat recovery analysis and the initial ORC modelling assumptions.

Figure 1a presents the simplified schematic of the ORC system considered in this study, and Fig. 1b depicts the associated Temperature-Duty (T-Q) sketch for the superheated subcritical process. Excluded from the schematic is a storage tank prior to the pump, and the bypass valve for the exhaust heat exchanger (exhaust side), the internal heat exchanger (high-pressure side) and the expansion machine. These components along with a control unit are required to enable the functioning of the system over a complete drive cycle.

The exhaust heat (A-B) is recovered in the exhaust heat exchanger (HEX), and the high-pressure pre-heated liquid is converted into superheated vapour (2-3). Assuming steady-state and steady-flow system, the energy transferred to the fluid (neglecting heat losses) is given as:

$$\dot{Q}_{HEX} = \dot{m}_{exh}\, c_p\, (T_A - T_B) \ldots (1)$$

Where, $\dot{Q}$ is the thermal duty (kW), $\dot{m}$ is the mass flow rate (kg/s), c_p is the specific heat (kJ/kg°C) and T is the temperature (K). Additionally, neglecting the kinetic and potential energies, the irreversibilities (internal and external combined) is calculated using the specific enthalpy and entropy of the fluid at the inlet (Pt. 2) and exit (Pt. 3) conditions, and the mean temperature of the heat source as [31]:

$$\dot{I}_{HEX} = T_{amb}\, \dot{m}_{fluid}\, [(s_3 - s_2) - \{(h_3 - h_2)/T_{exh\,mean}\}] \ldots (2)$$

Where, $\dot{I}$ is the irreversibilities (kW), s is the entropy (kJ/kg°C) and h is the enthalpy (kJ/kg). The temperature differences along A-B and 2-3 can be seen as a direct measure of irreversibilities.

The high-pressure superheated fluid is then passed through an expansion machine (3-4, dynamic or positive displacement). The work is transferred electrically (via generator) or mechanically (via gear train). The expansion and pumping processes are non-isentropic, and the power output is given as:

$$\dot{W}_{exp} = \dot{m}_{fluid}\, (h_3 - h_{4\,ideal})\, \eta_{exp} \ldots (3)$$

Where, $\dot{W}$ is the work done or absorbed (kW) and η is the isentropic efficiency. The expansion irreversibilities expressed using inlet (Pt. 3) and exit (Pt. 4) fluid conditions for the real expansion is calculated as:

$$\dot{I}_{exp} = T_{amb}\, \dot{m}_{fluid}\, (s_4 - s_3) \ldots (4)$$

To internally utilise the considerable exergy exiting the expansion machine, and hence avoid the potential loss in the condenser, an internal heat exchanger (IHE) is utilised. The vapour side (low-pressure side) of the IHE reduces the high-temperature low-pressure vapour exiting the expansion machine to a low-temperature low-pressure vapour prior to the condenser inlet (4-5). In doing so, the high-pressure low-temperature liquid exiting the pump (high-pressure side) recovers the enthalpy difference and is raised to a higher temperature (1-2). The internally transferred heat and the irreversibilities attributed to this process are calculated as:

$$\dot{Q}_{IHE} = \dot{m}_{fluid}\, c_p\, (T_4 - T_5) \ldots (5)$$

$$\dot{I}_{IHE} = T_{amb}\, \dot{m}_{fluid}\, [(s_5 - s_4) + (s_2 - s_1)] \ldots (6)$$

The fluid then rejects the heat to the air (C-D) and is converted from low-pressure vapour to sub-cooled liquid (5-6) in the condenser. The sub-cooling needs to be limited to a small amount to reduce the impact on the total condenser size. The energy transferred from the fluid and the condensing irreversibilities are calculated as:

$$\dot{Q}_{cond} = \dot{m}_{air}\, c_p\, (T_C - T_D) \ldots (7)$$

$$\dot{I}_{cond} = T_{amb}\, \dot{m}_{fluid}\, [(s_6 - s_5) - \{(h_6 - h_5)/T_{air\,mean}\}] \ldots (8)$$

To complete the closed-loop cycle, the sub-cooled liquid at the pump inlet is pressurised to enter the IHE (6-1). The power consumed by the pump and the pumping irreversibilities are calculated as:

$$\dot{W}_{pump} = \dot{m}_{fluid}\, (h_{1\,ideal} - h_6)/\eta_{pump} \ldots (9)$$

$$\dot{I}_{pump} = T_{amb}\, \dot{m}_{fluid}\, (s_1 - s_6) \ldots (10)$$

Finally, the net power ($\dot{W}_{net}$) and the thermal efficiency (η_I) are described as:

$$\dot{W}_{net} = \dot{W}_{exp} - \dot{W}_{pump} \ldots (11)$$

$$\eta_I = \dot{W}_{net}/\dot{Q}_{HEX} \ldots (12)$$

2.2 Rational for the reference

In automotive ORCs, negligible environmental impact and higher thermal stability requirements are considered essential for the chosen working fluid. Implementation of the mobile air-conditioning directive in the European Union led to the banning of R134a [32]. Such regulations in the future may also apply to automotive ORCs requiring the use of fluids with GWP less than 150. This may exclude the commercially popular R245fa, which is often suggested for stationary and marine ORCs [1, 11]. New selection criteria of low GWP and improving technologies to reduce flammability risks have led to a revived interest in using hydrocarbons and its derivatives [18, 33].

The thermal decomposition issue was primarily addressed in the literature using two avenues: firstly by using thermal-oil loops and secondly by using higher thermal stability fluids [18, 34]. Due to the additional size, complexity and weight (e.g. due to the gas-oil heat exchanger), thermodynamic (e.g. additional exergy destruction), and cost (estimated at an additional 20%) considerations, the thermal-oil loop approach was excluded as a potential solution in the considered application [9, 17]. It is stated that the molecular make-up of organic fluids fundamentally precludes the possibility of an ideal fluid [11, 35]. Nonetheless, the two fluids offering a preferred trade-off, and hence, proposed in the literature for high-temperature applications include toluene and MM [18, 36].

Figure 2 presents the net power results with increasing pressure for the commonly suggested high-temperature fluids utilising the modelling assumptions from Table 1. The maximum cycle pressure was normalised to the critical pressure. Although, these results are based on a non-constrained expansion machine size, nevertheless, the higher performance of toluene and MM validates the literature findings [6, 17]. The net power results for R245fa are also included, these were 35-50% lower than those of toluene and MM. The more complex fluids such as D5 and D6 were excluded from consideration due to freezing temperatures higher than -40°C. Freezing temperatures below -40°C (i.e. similar to the conventional engine coolant) are required for automotive applications. Furthermore, complex fluids are shown to offer lower thermodynamic performance and also exhibit technical constraints for expansion machine technology [17, 19]. Hence, toluene and MM cycles offer an appropriate reference for comparison for exploitation of exhaust heat. These two fluids offer the advantages of a relatively high thermal stability, high molecular weight, low GWP and the use of an IHE.

2.3 Parametric analysis

To demonstrate the cycle behaviour of an ORC with an IHE, two parametric studies are presented using toluene as an example: variation in maximum cycle pressure for dry saturated vapour expansion (Fig. 3a) and variation in maximum cycle temperature for fixed pressure expansion (Fig. 3b). This was so, since for assumed fixed condensing temperature, minimum pinch point temperature differences and isentropic efficiencies (Table 1), the cycle performance was primarily a function of the cycle pressure and the degree of superheat.

In both the cases, with either increasing pressure or superheat, the exhaust HEX duty decreased (due to pinch point limitation), while the IHE duty increased (due to increasing expansion exit enthalpy). As the IHE partially preheated the working fluid, the average heat addition temperature increased, which contributed towards the thermal efficiency increase [17]. With increasing pressure, a noticeable level of net power improvement was only observed up to a cycle pressure of 16 bar (Fig. 3a), whereas with increasing temperature, the net power decreased (Fig. 3b). Since the

context for ORC operation here is overall conversion efficiency (i.e. net power) rather than thermal efficiency, expansion inlet temperature just slightly above the dry saturated vapour temperature (i.e. 5 °C superheat) was chosen for the considered dry fluids.

Note that superheating under fixed evaporator and condenser pressures offered a system size advantage, i.e. reduction in expansion Volume Flow Ratio (VFR). The 60 °C superheat reduced the VFR from 17.4:1 to 16.5:1 (Fig. 3b). However, this advantage does not justifies neglecting the drawbacks of large superheating (e.g. increased system size). Furthermore, evaporators are typically designed to handle less than 10 % of the total load in vapour form. High superheating levels may then require the dedicated use of a superheater.

The parameters in Fig. 3a at 16 bar can also be used to illustrate how the IHE interaction affected the heat recovery, the net power and the condenser load compared to a simple ORC without IHE (where $\dot{Q}_{in} = \dot{Q}_{HEX} + \dot{Q}_{IHE}$). The cycle with an IHE utilised a smaller heat input (103 vs. 138 kW) for obtaining the same net power output (16.6 kW), hence it had a better thermal efficiency (16.2 vs. 12.1 %) and reduced the load on the air condenser (86 vs. 121 kW). The combined heat ($\dot{Q}_{HEX} + \dot{Q}_{IHE}$) used by the recuperated cycle was roughly constant to the net heat ($\dot{Q}_{in}$) into the non-recuperated cycle. This was because the presence of the IHE roughly compensated for the change in heat addition as a function of pressure and temperature. The net power was unchanged either with varying cycle pressure or with varying cycle temperature. This was because the specific work was only a function of pressure difference across the expansion. In summary, cycles with an IHE decreased the heat recovery efficiency, had no impact on the net power, and hence, decreased the condenser load. Note the exclusion of low-temperature heat recovery is an advantage for exhaust heat recovery, but not for the heat streams that are already a load on the engine cooling module.

2.4 Size and performance trade-off

In order to quantify the practical performance improvement potential using toluene and MM, a size and performance trade-off study was conducted for the four major system components. These being the size of the expansion machine, the exhaust heat exchanger, the internal heat exchanger and the air condenser. As a first approximation, the following was considered as an indicator of relative size variation for a heat transfer component. It was assumed that the overall heat transfer coefficient (U, W/m^{2}°C) remained relatively unchanged for a particular fluid under a fixed process type. Therefore, UA (W/°C), where A (m^2) is the heat transfer area, was considered as an indicator for the relative heat transfer size. Similarly, the VFR of the expansion machine was considered as an indicator of the relative expansion machine size for a particular fluid under a fixed process type.

Figure 4a shows the influence of the VFR on the net power. The maximum net power for toluene was achieved at a high VFR value of 40:1. However, such levels of VFRs are beyond the reach of any efficient single-stage expansion machine. As a trade-off, the design point VFR was reduced to 14:1. This was so, since the net power improvement with VFRs above this value was relatively insignificant to justify the added design intensity, size and the associated costs. A similar trade-off approach for MM resulted in a design point VFR of 12:1.

Figure 4b shows the influence of the exhaust heat exchanger *UA* values on the net power. There is a region beyond which the *UA* values increased for a negligible improvement in power. This region corresponded to a minimum pinch point temperature difference of 25-35 °C for both the fluids. Since an ideal IHE has no impact on the expansion power, Fig. 4c shows that the figure of merit to assess the impact of IHE was the cycle thermal efficiency. *UA* values corresponding to pinch point value of 10 °C for both the fluids were considered near-optimal.

Finally, Fig. 4d shows the influence of the air condenser *UA* value on the net power. A realistic trade-off with this component is one of the vital modelling assumptions, since the performance of any fluid bottoming cycle is very sensitive to the heat rejection limit. Additionally, overly optimistic condensing temperatures cannot be considered as a norm with the existing demands on the modern engine cooling module. Assuming the addition of an air cooled ORC condenser after the engine radiator, the temperature of the available cooling air was then 40 °C (Fig. 5). By limiting the air in the engine bay to 60 °C, the near-optimal region then corresponded to an average design condensing temperature of 70 °C for both the fluids (Fig. 4d). To give an appreciation of the challenge this brings to the engine manufacturers and original equipment suppliers, Fig. 5 shows the relative size of the various heat transfer elements in the engine cooling module based on their thermal duty at B100.

Table 2 summarises the key system, size and design intensity, and performance parameters for toluene and MM cycles based on the fixed design point values selected in Fig. 4. Note that, selecting larger *UA* and VFR values will reduce the heat transfer irreversibility and increase the performance, respectively, but will have a negative impact on system packaging and cost. It was seen that the toluene and MM cycles were 11.1-13.4 % thermally efficient, and could potentially offer an additional 4-4.7 % of engine power. MM and toluene both required high VFRs (12:1, 14:1) making them better suited to large single-stage radial turbines and piston expanders [37].

3 Problem definition for the conventional ORC

The potential overall fuel consumption improvements using toluene and MM cycles can play a significant part in achieving the impending fuel consumption regulations. However, the conventional ORC approach for exhaust heat recovery is still not reaching the required fuel savings within the expected costs. Since ORC systems are only 10-15 %

283 efficient, considering the irreversibilities in the ORC may offer a focused research direction in improving the
284 performance and cost-effectiveness of the system at a very fundamental level. For this consider Fig. 6, which presents
285 the component irreversibility contributions in the design point toluene cycle. It is seen that the HEX made the highest
286 contribution (40 %, 12 kW), closely followed by the condenser (29 %, 8.7 kW), and then by the expander
287 (19 %, 5.6 kW). Contributing to the high heat transfer irreversibilities was the near isothermal phase-change and the
288 high condensing temperature. The relatively high irreversibility contribution due to the expander was related to the
289 realistic isentropic efficiency of 65 %. The irreversibility equations presented in Section 2.1 were utilised to produce
290 Fig. 6.
291
292 A means to address the heat transfer irreversibility drawbacks in the literature was by employing a supercritical cycle,
293 especially using ethanol [38]. A supercritical cycle offers lower HEX irreversibilities, since it avoids near isothermal
294 evaporation, and allows the exclusion of the IHE, since the IHE duty decreases with increasing pressure for a fixed
295 maximum temperature [9]. Nonetheless, under high source temperatures (≈ 400 °C) and high source-to-sink
296 temperature differentials (≈ 350 °C), this is typically challenging in practice due to the excessive system pressures
297 (> 65 bar, ethanol) and the need for high expansion VFRs (> 40:1, ethanol) [9, 17].
298
299 Toluene and MM cycles have sub-atmospheric condensing pressures at typical engine radiator temperature levels
300 (85-95 °C). In addition, the use of an IHE introduces additional controls, hardware, complexity and cost for the ORC
301 system. Despite these challenges, the concept of internal heat recuperation is particularly useful for automotive
302 exhaust heat recovery to limit the size of the additional air-cooled condenser in an already demanding engine cooling
303 module. The above discussion (Fig. 2 and Table 2) then indicates that alternative avenues, which attempt to retain the
304 favourable characteristics of toluene and MM, while offering superior performance, remain a theme of investigation.
305 Note that due to a lower performance potential and thermal stability concern, blends with significant R245fa and
306 n-pentane concentrations as suggested by Le et al., were not considered in the current case [39].
307
308 **4 Proposed ORC**
309 **4.1 Method overview**
310 To improve the case for ORCs, a study was undertaken to identify methods that would translate to noticeable benefits.
311 An identified path was to formulate novel organic fluid blends with unique heat transfer and expansion characteristics,
312 while retaining Toluene and MM as a noticeable blend component. Such a research direction is novel to the current
313 research trends in the automotive sector, which are typically aimed towards component development and
314 improvements in component efficiencies to make the ORC systems cost-effective [4, 18]. Although, efficient HEXs and

315 high VFR expansion machines will be vital in the deployment of ORC systems, these approaches only indirectly
316 address the fundamental cycle drawbacks.
317
318 The blend screening methodology, presented in Table 3, was developed and applied to examine over 225
319 documented Toluene and MM blends [40-42]. It has been shown that an incorrect selection of the blend may result in
320 poorer thermodynamic and economic performance over the pure fluid counterpart [43]. Hence, extending upon the
321 earlier studies, the current screening methodology consisted of 22 criteria [9, 27]. To illustrate the primary screening
322 criteria, Fig. 7b presents the hypothetical T-S sketch of the desired ORC. This is contrasted to Fig. 7a, which depicts
323 the hypothetical T-S sketch of a conventional ORC. The improved expansion and the unique heat transfer
324 characteristics, which collectively can offer an improved energy conversion concept and a higher energy density
325 solution are summarised below:
326 - Property 1 and/or 2: An increased latent heat (i.e. reduced mass flow rate) and/or a higher vapour density at the
327 minimum cycle pressure. This increases the system temperature and pressure differential for a fixed expansion
328 machine size.
329 - Property 3: A low temperature variation during condensation to mirror a low heat sink temperature rise. This
330 reduces the heat transfer irreversibilities and offers lower average condensation temperatures.
331 - Property 4: A high temperature variation during evaporation to mirror the high heat source temperature drop. This
332 reduces the heat transfer irreversibilities and increases the average heat addition temperature.
333 - Property 5: Retention of high concentration of Toluene and MM. This attempts to retain the advantages associated
334 with higher molecular weight, higher thermal stability and internal heat recuperation.
335
336 The screening results were limited to the selection of just one blend each for Toluene and MM by marginally tightening
337 the initial screening criteria. The two resulting blends were termed T80 and MM80, based on toluene and MM
338 percentage by mass, e.g. T80 corresponding to 80 % toluene. An attempt is made in Section 4.4 to compare the
339 relevant blend properties using the recommended fluid property packages. Additionally, the Vapour-Liquid Equilibrium
340 (VLE) behaviour was validated against the available numerical and/or experimental data [40-42, 44]. For example,
341 Fig. 8 shows the VLE behaviour of T80 at 10 bar within the 2 °C error criterion for a minimum of 10 data sets
342 (property 6). Note that, the second blend constituents will be disclosed in a subsequent article, following
343 experimentation. A further consideration in the selection of the blend constituents was the high availability in the
344 market place, and a demonstrated use in the chemical and process industries (property 7).
345
346 It is important to highlight that the evaporation and condensation characteristics of the proposed blend (Fig. 7b) are
347 different to the typical approach of using a zeotropic blend (hypothetical T-S sketch presented in Fig. 7c). This is so,

since the proposed blend is a pressure swing blend, i.e. one in which the composition at which the azeotrope occurs changes with the pressure (property 8). Hence, for a fixed composition, different temperature glides are possible in different heat transfer equipment's, whereas a zeotropic fluid offers similar temperature glides in the evaporation and condensation processes, and usually do not include the considerations relating to the expansion VFR. Comparing the 3 hypothetical T-S sketches, it can be concluded that the proposed blend can offer higher overall conversion efficiency when compared to the conventional pure fluid and zeotropic blend options. The justifications for the remaining screening parameters relevant to the present application are provided during the discussions in the following sub-sections.

4.2 Results and discussion

As a preliminary step to the detailed heat transfer equipment and expansion machine models, the following was considered for size and design intensity similarity between the pure fluid and its blend. It was assumed that, *U* was similar for the pure fluid and its blend. This assumption was made due to the high mass fraction of the original pure fluid (property 5), and screening of improved thermal conductivity (property 9) and specific heat values (property 10) for the blend constituent. Therefore, *UA* was considered equal for the pure fluid and its blend to act as an indicator of similar HEX, IHE and condenser sizes. Similarly, VFR defined as the ratio between the volumetric flow rates at the expansion outlet to inlet was also considered equal to act as an indicator of similar expansion machine size.

Table 2 also summarises the system, size and design intensity, and performance parameters for T80 and MM80. For an equivalent heat transfer footprint and expansion machine size, T80 offered approximately 20 % improvement in thermal efficiency (13.4 vs. 16.2 %) and net power (14.8 vs. 18 kW). This net power corresponded to a 5.7 % improvement in the overall BTE from 41.4 to 43.8 %. Similarly, MM80 offered approximately 25 % improvement in thermal efficiency (11.1 vs. 13.9 %) and net power (12.6 vs. 15.6 kW). Contrary to the pure fluids, the blends offered super atmospheric condensation pressures. This was so since, the formulated blends were homogeneous positive azeotropes and their boiling points were lower than both of the blend constituents (property 8 and 11). As a result, the blends will demonstrate a lower sensitivity to the absolute pressure loss in any heat transfer element. This advantage bodes well for the use of inexpensive heat transfer equipment for the blends. Hence, the high boiling point of the higher thermal stability fluids was one of the reasons that drove the organic blend study.

Figure 9a and b depicts the T-S diagram of toluene and T80 for comparison under an equivalent size and design intensity. T80 offered a 57 and 34 °C temperature differences during evaporation and condensation processes, mirroring the high heat source temperature drop (251 °C) and the low heat sink temperature rise (20 °C), respectively. Similarly, MM is compared to MM80 in Fig. 9c and d, where MM80 offered a 29 and 15 °C glides during evaporation

and condensation processes, respectively. In both cases, the pure fluid and its blend recovered nearly equal amounts of exhaust heat. However, the blends offered higher pressure (22.7 vs. 8.8; 16.9 vs. 7.5 bar) and temperature (182 vs. 151; 141 vs. 128 °C) differentials in the cycle. In all the cases, the maximum working fluid temperature was below 250 °C. To minimise the numerical error in the *UA* value for the blends the heat exchange was divided into 10 equal enthalpy intervals during the phase-change process.

Both the blends allowed the continued use of the IHE, which is vital for reducing the size of the air cooled condenser. For the considered IHE, the pinch point for all the fluids occurred close to the low-temperature low-pressure vapour side and the high-pressure low-temperature liquid side. The IHE duty for toluene and T80 both corresponded to approximately 30 % of the total heat input. However, the IHE duty for MM was higher at approximately 60 %, compared to 45 % for MM80. The IHE duty is a function of the ratio of latent heat to sensible heat, the level of superheat, the shape of the saturated vapour curve, the condensing temperature and the expansion efficiency. The IHE duty for MM80 was lower since the screening criteria avoided the formulation of extremely drying blends with low latent heat of vaporisation (property 1 and 12). The concept of internal heat recuperation is advantageous, however in reality, due to the nature of organic-vapour to organic-liquid heat exchange process, the heat transfer coefficients are relatively low. Hence, a trade-off exists even between the level of internal heat recuperation and size [17].

A concern with blends offering significant glide (i.e. both pressure swing and zeotrope) in practical application is that under reduced source heat in the evaporator the lower boiling point fluid will boil and float to the top entering the expansion machine first. This may lead to the accumulation of the higher boiling point fluid, bringing challenges such as incomplete phase change (i.e. two-phase at the expansion machine inlet) and decreased heat transfer performance. Nevertheless, since the blends were formulated to recover high grade heat, this issue may be addressed by using a slightly superheated expansion, as simulated here, rather than dry saturated vapour expansion. A marginal superheat in the evaporator will ensure all the constituents are evaporated and the relative mass ratios are maintained.

4.3 Rational for the blend composition

The 80 % by mass concentration of toluene and MM were considered as near-optimal. Consider Fig. 10a, which compares the turbine size parameter (S_{exp}, m) and UA/kW value for varied toluene concentration as calculated using the below equations.

$$S_{exp} = \sqrt{\dot{V}_{exit}}/\Delta h_{exp}^{0.25} \ldots (13)$$

$$UA/kW = (UA_{EXH} + UA_{IHE} + UA_{cond})/\dot{W}_{net} \ldots (14)$$

Where, $\dot{V}$ is the volume flow rate (m^3/s). The physical significance of S_{exp} and UA/kW values are given by the proportionality to the actual turbine dimensions and normalised overall heat transfer footprint, respectively [19, 45]. The ORC was modelled utilising the assumptions in Table 1 and was targeted for an equal net power of 13 kW by varying the cycle pressure.

The 80% toluene concentration demonstrated the lowest UA/kW value (i.e. 23% lower than T20). For these concentrations, the variation in the turbine size was relatively low (i.e. 6% between T80 and T20). Furthermore, Fig. 10b compares the thermal efficiency for the varied toluene concentration. T80 demonstrated the highest thermal efficiency (i.e. 12% higher than T20). Contributing to the higher thermal efficiency was the efficient heat exchange in the IHE and around twice the temperature glide in the ideal evaporation process compared to the ideal condensation process (i.e. without pressure losses). Hence, when considering the turbine size parameter, UA/kW value and thermal efficiency, the 80% toluene concentration offered a preferred blend. The same was also true for the selection of 80% MM concentration. The higher concentration was additionally chosen to retain the advantages of higher molecular weight and higher thermal stability (property 5). A higher molecular weight bodes well for turbines as expansion machines. Since, a single method to reintroduce the recovered energy into the powertrain has not yet been identified by the HDDE sector, the use of T80 and MM80 may allow the continued examination of both radial turbines and piston expanders.

4.4 Fluid properties

Table 4 presents the key fluid properties for comparison between the blends and their pure fluid counterparts. The values are presented for a low-temperature saturated-liquid condition and a high-temperature saturated-vapour condition. This offers an indication about the various fluid properties at the two possible extreme temperature, pressure and phase conditions that may be experienced in an ORC. At the low-temperature condition, the blends offered marginal improvements in thermal conductivity (5%) and specific heat (18%). Whereas, at the high-temperature condition, the specific heat values were nearly equal and the thermal conductivity was marginally higher for the blends (9%). As a first approximation, these results support the equivalent *U* assumption made in this study between the blend and its pure fluid counterpart. The pure fluid and blend properties were calculated using the Peng-Robinson and Wilson fluid property packages, respectively [46].

Furthermore, due to the screening criteria employed (Table 3), the blends are expected to offer freezing temperatures (property 13), thermal decomposition temperatures (property 14), auto-ignition temperatures (property 15), National Fire Protection Association rating (property 16, 17 and 18) and environmental impact (property 19 and 20) comparable to the pure fluid counterparts, so as to retain their validity for the considered application [9, 17, 35, 47]. The blends are

additionally expected to offer the carryover of the currently developed ORC components for hydrocarbons and siloxanes. This is expected due to the molecular makeup (property 21) and a wide compatibility with common metals and alloys, O-ring materials and thermoplastic (property 22) as the additional screening criteria for the blend constituent [9, 48] .

5 Economic analysis

The current market niche for ORC systems is dependent on simplicity and affordability, with initial technology deployment on automotive HDDEs expected during the middle of the next decade. To estimate the potential cost savings when utilising the identified blends over their pure fluid counterparts, a detailed economic review and an original cost analysis study was conducted. In the detailed economic review, appropriate equations representing the conceptual equipment cost estimates were derived from references [6, 30, 39, 49-52]. Whereas, in the original cost analysis study, a significant volume of equipment cost and capability data was collected during a pre-procurement research phase from the north American and the European process industry supply chain. As a result of these two studies, purchase cost equations (in USD) for all the major ORC components were formulated, as presented in Table 5. These were under the assumptions of high volumes of production, direct exhaust heat utilisation and output capacities of 10-100 kW. Applying the chemical engineering plant cost index, the equations were adjusted to the end of the year 2015. A further marginal adjustment was included to account for the cost and capability improvements due to the current technological advancements resulting from the findings of the original cost analysis study. However, the effect of this was limited to less than a 20 % variation over the equations representing the conceptual equipment costs. Note that, these equations are corrected and must be utilised within the range of application stated.

Such cost estimating methodologies are considered valuable in feasibility studies. By considering the key design and operational characteristics of a process, not only the competitive position may be assessed, but this may also aid in focussing the development efforts. These equations were based on the step count and exponential methods for order-of-magnitude estimates derived from commercial data. Although the actual cost of a particular equipment depends on multiple factors, nonetheless, cost functions can be linked to some key variables to provide estimates with errors as low as 10 %. For the considered case, these variables included, materials of construction, operating conditions (i.e. pressure, temperature and phase) and parameters relating to the capacity (i.e. power, area and volumetric flow). Note that, for some processes, two suitable types of equipment's were available, and hence, two cost equations were considered. They were grouped as primary and secondary options, based on the number of dependent variables. To avoid over simplification, the primary options were typically a function of one additional variable compared to the secondary option. For example, the blends required higher pressures (10-15 bar) than their pure fluid counterparts. Hence, the cost equations corresponding to the primary ORC option accounted for the

increased costs due to this variable. Whereas, in the secondary ORC option, the components had no cost variation under the considered pressure range.

Table 6 presents the cost results for the blends and their pure fluid counterparts for the primary and secondary ORC options. The pipe length (7.5 m) and diameter (0.015 m), the tank capacity (30 L), and the expansion machine bypass valve diameter (0.015 m) were considered equal for all the fluids. Furthermore, the control and instrumentation ($ 900), and the unaccounted hardware costs ($ 900) were also considered equal. For ORCs under the considered application, these five items accounted only 0.5-2.5 % each of the total system cost. Therefore, the above fixed cost assumptions should give sufficient accuracy, since their impact on the overall cost variation between the different fluids will be marginal. The quotations for the identified blends and their pure fluid counterparts were sourced from two different suppliers each, for quantities representing near economies-of-scale (Sigma Aldrich, Fisher Scientific, Spectrum Chemical, TCI Chemical). The resulting fluid costs were 5.1, 6.8, 7.5 and 10.8 $/L for toluene, MM80, MM and T80, respectively. A fixed 30 L fluid cost was added for each of the ORC options.

To estimate the required area for the HEX, the IHE and the condenser, mean *U* values were considered for exhaust to evaporating-hydrocarbons (65 W/m^2°C), vapour-hydrocarbons to liquid-hydrocarbons (200 W/m^2°C) and air to condensing-hydrocarbons (475 W/m^2°C) from references [5, 51-53], respectively. The same set of values were utilised for both the blends and their pure fluid counterparts. These values are only meant to act as a reference for comparison between the pure fluid and its blend (e.g. Toluene vs. T80) due to the comparable heat transfer properties (Table 4). They are not suggested for comparing two noticeably different fluids (e.g. Toluene vs. MM), which may require detailed heat transfer equipment design.

From table 6, it can be noted that on average, the turbine-generator unit had the highest proportional cost (45 %), followed by the air cooled condenser (25 %) and finally by the exhaust HEX (12 %). The cost of the air cooled condenser included the cost of an additional fan and motor, while the exhaust HEX costs were based on evaporator type HEXs for direct high-temperature exhaust heat utilisation. The pump and IHE costs were relatively similar at 5% each. The thermodynamic and economic optimisation study by Le et al. has also indicated the highest proportional cost (approximately 40 %) due to the turbine-generator unit [39]. As a result, in exhaust heat recovery applications, which correspond to high-temperature differentials between the heat source and the heat sink, the requirement of cost-effective and efficient piston expanders with high VFRs remains a vital development direction.

The total absolute ORC costs when utilising the identified blends were marginally higher (2-3 %) compared to their pure fluid counterparts. Fig. 11a shows the marginally higher absolute cost for the T80 cycle when compared to the

toluene cycle for the primary option. This was principally due to the turbine-generator (5% due to higher capacity), the exhaust HEX (3% due to higher pressure) and the pump (13% due to higher pressure) costs. Similarly, Fig. 11c shows the marginally higher absolute cost for the T80 cycle when compared to the toluene cycle for the secondary option. In the secondary ORC option, the pump and the exhaust HEX costs were not a function of the variation in the demonstrated range of pressure. As a result, the cost of the turbine-generator increased (5% due to higher capacity), however, the exhaust HEX costs were equal, while the pump cost decreased (7% due to lower volumetric flow).

To estimate the relative techno-economical trade-off between the blends and their pure fluid counterparts, the total system cost per unit of net power ($/kW) value was considered. A relative comparison between ORCs will be more accurate when comparable working fluids (molecular make-up, property 21) under similar operating conditions (slightly superheated subcritical operation, Table 2) are considered. Furthermore, the blends offered marginal improvements in the expansion exit density (10-50%, Table 2), which additionally support the assumptions in the cost analysis [49]. As shown in Table 2, the blends demonstrated 22-24% higher net power. Therefore, when considering the $/kW value as a measure, the blends demonstrated a 15-18% improvement. Fig. 11b shows a 15% reduction in the $/kW value for the T80 cycle when compared to the primary toluene cycle option. Note that the secondary ORC option utilised pump, exhaust HEX and IHE that were approximately 50% lower in cost compared to the primary ORC option (i.e. nearly $4750 in total). As a result, the secondary T80 cycle option presented the lowest $/kW value of 1792. This was 16% lower than that demonstrated by the secondary toluene cycle option (Fig. 11d).

It is important to highlight that since the resulting absolute component costs were derived from the process industries, they may not represent the true cost that can be demonstrated by the automotive sector. Preliminary and confidential cost data available from automotive consortiums indicated that the absolute cost of some of the prototype components may be up to 50% lower than those presented here [9, 54]. This is principally due to the synergies with the current automotive components, for example, adapting exhaust gas recirculation coolers to exhaust HEXs and turbocharges to turbines. Nonetheless, the analysis presented here is valuable in evaluating the relative cost variation amongst the options. Finally, despite the increased design intensity and cost of high-temperature ORCs (>400°C), the $/kW values of the chosen blends under the primary option agree within a range of 10-20% when compared to the low-temperature ORCs studies (<200°C) using hydrocarbons (e.g. n-butane and n-pentane) from the literature [39, 49].

Note that, parameters like the net power per unit of heat transfer area may not be a suitable indicator for the relative cost comparison in the considered application and capacity range [12, 45]. This is so since, heat transfer costs typically accounted for only 40% of the overall system cost. Net power per unit of heat transfer area may be better

suited to larger scale ORC units for lower grade heat recovery where the heat exchanger sizes and costs can be a dominant factor.

6 Conclusion

The use of toluene and MM as working fluids in high-temperature ORCs appears to be the preferred approach in the literature. However, these conventional ORCs are not reaching the required fuel savings within the expected costs for automotive applications. To facilitate the introduction of ORCs, an innovative approach has been presented in this paper. The concept aims to offer an efficient thermal match to the source and sink streams, increase the system temperature and pressure differentials, and decrease the sensitivity to system pressure losses. These advantages were achieved by adapting the fluid makeup using novel blends based on the developed 22 criteria screening methodology. Blends were formulated with toluene and MM as the significant component, so as to retain higher thermal stability, high molecular weight, low environmental impact and efficient use of an IHE. Two blends, one containing 80% toluene by mass (T80) and the other containing 80% MM by mass (MM80) were identified as near-optimum. These blends offered varying levels of temperature glides in the exhaust HEX and the air condenser to address the irreversibility losses due to isothermal phase-change at subcritical pressures. The blends also offered higher density at the minimum cycle pressure with reduced mass flow rate to increase the system temperature and pressure differentials for fixed expansion volume flow ratios.

Simulations conducted for an equivalent heat transfer footprint (approximated as *UA*) and expansion machine size (approximated as VFR) amongst the blends and their pure fluid counterparts demonstrated a 20-25% improvement in thermal efficiency and net power. As a result, the proposed ORC approach utilising the blends presented the advantage of 15-18% lower $/kW value compared to the pure fluid counterparts, thus improving commercialisation potential. The economic analysis was based on the step count and exponential methods for order-of-magnitude estimates derived from the latest commercial data. Under realistic boundary conditions and assumptions for automotive HDDEs, a maximum of 5.7% improvement in the overall engine BTE was achieved, with the most competitive ORC option costing 1792 $/kW.

The higher energy-density and cost-effective ORC approach presented in this paper was investigated using a simulation tool (Aspen HYSYS V8). Limited but crucial parameters were selected to offer a first basis for comparison. Additionally, appropriate equation-of-state was utilised to determine the blend characteristics. To address the limitations of this study, future works will focus on detailed heat exchanger and expansion machine models, followed by experimental results. Furthermore, since the charge air cooling has become a significant load on the modern engine cooling module, integration of this heat source will be investigated for transient conditions.

Acknowledgements

The author would like to acknowledge the support of Daniel Coren and the Advanced Engineering Centre with respect to proof-reading and provision of software tools, respectively.

Reference

[1] T. Wang, Y. Zhang, Z. Peng, G. Shu, A review of researches on thermal exhaust heat recovery with Rankine cycle, Renewable and Sustainable Energy Reviews, 15 (2011) 2862-2871.

[2] C. Sprouse III, C. Depcik, Review of organic Rankine cycles for internal combustion engine exhaust waste heat recovery, Appl Therm Eng, 51 (2013) 711-722.

[3] S. Edwards, J. Eitel, E. Pantow, P. Geskes, R. Lutz, J. Tepas, Waste Heat Recovery: The Next Challenge for Commercial Vehicle Thermomanagement, SAE Int. J. Commer. Veh., 5 (2012) 395-406.

[4] D.W. Stanton, Systematic Development of Highly Efficient and Clean Engines to Meet Future Commercial Vehicle Greenhouse Gas Regulations, SAE Int. J. Engines, 6 (2013) 1395-1480.

[5] A. Domingues, H. Santos, M. Costa, Analysis of vehicle exhaust waste heat recovery potential using a Rankine cycle, Energy, 49 (2013) 71-85.

[6] A.S. Nafey, M.A. Sharaf, Combined solar organic Rankine cycle with reverse osmosis desalination process: Energy, exergy, and cost evaluations, Renew Energ, 35 (2010) 2571-2580.

[7] M. He, X. Zhang, K. Zeng, K. Gao, A combined thermodynamic cycle used for waste heat recovery of internal combustion engine, Energy, 36 (2011) 6821-6829.

[8] H. Chen, D.Y. Goswami, E.K. Stefanakos, A review of thermodynamic cycles and working fluids for the conversion of low-grade heat, Renewable and Sustainable Energy Reviews, 14 (2010) 3059-3067.

[9] A. Panesar, Waste Heat Recovery Using Fluid Bottoming Cycles For Heavy Duty Diesel Engines, PhD. thesis. School of Computing, Engineering and Mathematics, University of Brighton, DOI: 10.13140/RG.2.1.4559.0248, 2015.

[10] B.F. Tchanche, G. Lambrinos, A. Frangoudakis, G. Papadakis, Low-grade heat conversion into power using organic Rankine cycles - A review of various applications, Renewable and Sustainable Energy Reviews, 15 (2011) 3963-3979.

[11] U. Larsen, L. Pierobon, F. Haglind, C. Gabrielii, Design and optimisation of organic Rankine cycles for waste heat recovery in marine applications using the principles of natural selection, Energy, 55 (2013) 803-812.

[12] F. Yang, H. Zhang, C. Bei, S. Song, E. Wang, Parametric optimization and performance analysis of ORC (organic Rankine cycle) for diesel engine waste heat recovery with a fin-and-tube evaporator, Energy, 91 (2015) 128-141.

[13] Z. Dimitrova, P. Lourdais, F. Maréchal, Performance and economic optimization of an organic rankine cycle for a gasoline hybrid pneumatic powertrain, Energy, 86 (2015) 574-588.

610 [14] S. Lecompte, H. Huisseune, M. van den Broek, M. De Paepe, Methodical thermodynamic analysis and regression
611 models of organic Rankine cycle architectures for waste heat recovery, Energy, 87 (2015) 60-76.
612 [15] M. Imran, B.-S. Park, H.-J. Kim, D.-H. Lee, M. Usman, Economic assessment of greenhouse gas reduction
613 through low-grade waste heat recovery using organic Rankine cycle (ORC), Journal of Mechanical Science and
614 Technology, 29 (2015) 835-843.
615 [16] M.-H. Yang, R.-H. Yeh, Thermodynamic and economic performances optimization of an organic Rankine cycle
616 system utilizing exhaust gas of a large marine diesel engine, Appl Energ, 149 (2015) 1-12.
617 [17] F.J. Fernández, M.M. Prieto, I. Suárez, Thermodynamic analysis of high-temperature regenerative organic
618 Rankine cycles using siloxanes as working fluids, Energy, 36 (2011) 5239-5249.
619 [18] D. Seher, T. Lengenfelder, J. Gerhardt, N. Eisenmenger, M. Hackner, I. Krinn, Waste Heat Recovery for
620 Commercial Vehicles with a Rankine Process, 21st Aachen Colloquium Automobile and Engine Technology, October
621 8-12, Aachen, Germany, 2012.
622 [19] D. Maraver, S. Quoilin, J. Royo, Optimization of Biomass-Fuelled Combined Cooling, Heating and Power (CCHP)
623 Systems Integrated with Subcritical or Transcritical Organic Rankine Cycles (ORCs), Entropy, 16 (2014) 2433-2453.
624 [20] Y.-Q. Zhang, Y.-T. Wu, G.-D. Xia, C.-F. Ma, W.-N. Ji, S.-W. Liu, K. Yang, F.-B. Yang, Development and
625 experimental study on organic Rankine cycle system with single-screw expander for waste heat recovery from
626 exhaust of diesel engine, Energy, 77 (2014) 499-508.
627 [21] H. Wang, R. Peterson, K. Harada, E. Miller, R. Ingram-Goble, L. Fisher, J. Yih, C. Ward, Performance of a
628 combined organic Rankine cycle and vapor compression cycle for heat activated cooling, Energy, 36 (2011) 447-458.
629 [22] A. Yılmaz, Transcritical organic Rankine vapor compression refrigeration system for intercity bus air-conditioning
630 using engine exhaust heat, Energy, 82 (2015) 1047-1056.
631 [23] G. Shu, J. Zhao, H. Tian, X. Liang, H. Wei, Parametric and exergetic analysis of waste heat recovery system
632 based on thermoelectric generator and organic rankine cycle utilizing R123, Energy, 45 (2012) 806-816.
633 [24] G. Yu, G. Shu, H. Tian, H. Wei, L. Liu, Simulation and thermodynamic analysis of a bottoming Organic Rankine
634 Cycle (ORC) of diesel engine (DE), Energy, 51 (2013) 281-290.
635 [25] E.H. Wang, H.G. Zhang, Y. Zhao, B.Y. Fan, Y.T. Wu, Q.H. Mu, Performance analysis of a novel system
636 combining a dual loop organic Rankine cycle (ORC) with a gasoline engine, Energy, 43 (2012) 385-395.
637 [26] C. Yue, D. Han, W. Pu, Analysis of the integrated characteristics of the CPS (combined power system) of a
638 bottoming organic Rankine cycle and a diesel engine, Energy, 72 (2014) 739-751.
639 [27] A.S. Panesar, R.E. Morgan, N.D. Miché, M.R. Heikal, Working fluid selection for a subcritical bottoming cycle
640 applied to a high exhaust gas recirculation engine, Energy, 60 (2013) 388-400.
641 [28] Aspen Technology Software, HYSYS version 8, 2015.
642 [29] Ricardo Software, WAVE version 8.1, 2015.

643 [30] D. Meinel, C. Wieland, H. Spliethoff, Economic comparison of ORC (Organic Rankine cycle) processes at
644 different scales, Energy, 74 (2014) 694-706.
645 [31] P.J. Mago, L.M. Chamra, K. Srinivasan, C. Somayaji, An examination of regenerative organic Rankine cycles
646 using dry fluids, Appl Therm Eng, 28 (2008) 998-1007.
647 [32] European Parliament, Directive 2006/40/EC of the European Parliament relating to emissions from air
648 conditioning systems in motor vehicles.
649 [33] Underwriters Laboratories, White Paper: Revisiting Flammable Refrigerants, 2011.
650 [34] G.Q. Shu, G. Yu, H. tian, H. Wei, X. Liang, Simulations of a Bottoming Organic Rankine Cycle (ORC) Driven by
651 Waste Heat in a Diesel Engine (DE), SAE International, 10.4271/2013-01-0851, 2013.
652 [35] J.M. Calm, G.C. Hourahan, Physical, Safety, and Environmental Data Summary for Current and Alternative
653 Refrigerants, International Congress of Refrigeration, August 21-26, Prague, Czech Republic, 2011.
654 [36] M.A. Siddiqi, B. Atakan, Alkanes as fluids in Rankine cycles in comparison to water, benzene and toluene,
655 Energy, 45 (2012) 256-263.
656 [37] G. Latz, S. Andersson, K. Munch, Selecting an Expansion Machine for Vehicle Waste-Heat Recovery Systems
657 Based on the Rankine Cycle, SAE International, 10.4271/2013-01-0552, 2013.
658 [38] H. Teng, G. Regner, C. Cowland, Achieving High Engine Efficiency for Heavy-Duty Diesel Engines by Waste Heat
659 Recovery Using Supercritical Organic-Fluid Rankine Cycle, SAE International, 10.4271/2006-01-3522, 2006.
660 [39] V.L. Le, A. Kheiri, M. Feidt, S. Pelloux-Prayer, Thermodynamic and economic optimizations of a waste heat to
661 power plant driven by a subcritical ORC (Organic Rankine Cycle) using pure or zeotropic working fluid, Energy, 78
662 (2014) 622-638.
663 [40] DDBST, Online Dortmund Data Bank Search, ddbst.com/ddb-search.html, Accessed on 07.07.2015.
664 [41] L.H. Horsley, Azeotropic Data-III, Volume 3, American Chemical Society, ISBN 9780841205338, 1973.
665 [42] D.R. Lide, H.V. Kehiaian, CRC Handbook of Thermophysical and Thermochemical Data, Volume 1, Taylor &
666 Francis, ISBN 9780849301971, 1994.
667 [43] Y. Feng, T. Hung, K. Greg, Y. Zhang, B. Li, J. Yang, Thermoeconomic comparison between pure and mixture
668 working fluids of organic Rankine cycles (ORCs) for low temperature waste heat recovery, Energ Convers Manage,
669 106 (2015) 859-872.
670 [44] CHERIC, Binary Vapor-Liquid Equilibrium Data, cheric.org/research/kdb, Accessed on 07.07.2015.
671 [45] H. Tian, G. Shu, H. Wei, X. Liang, L. Liu, Fluids and parameters optimization for the organic Rankine cycles
672 (ORCs) used in exhaust heat recovery of Internal Combustion Engine (ICE), Energy, 47 (2012) 125-136.
673 [46] Aspen HYSYS V8, Physical Property Methods, 2015.
674 [47] R. Chacartegui, D. Sánchez, J.M. Muñoz, T. Sánchez, Alternative ORC bottoming cycles FOR combined cycle
675 power plants, Appl Energ, 86 (2009) 2162-2170.

[48] J.M. Calm, Air-Conditioning and Refrigeration Technology Institute Refrigerant Database, Data Summaries: Volume 1, 2, 3: Single-compound Refrigerants, Zeotropes and Azeotropes, Toxicity and Compatibility (DOE/CE/23810-105,106,107), Virginia, U.S, 1999.

[49] S. Quoilin, S. Declaye, B.F. Tchanche, V. Lemort, Thermo-economic optimization of waste heat recovery Organic Rankine Cycles, Appl Therm Eng, 31 (2011) 2885-2893.

[50] R.K. Sinnott, Chemical Engineering Design: Chemical Engineering, Volume 6, Elsevier Science, ISBN 9780080492551, 2005.

[51] R.H. Perry, D.W. Green, Perry's Chemical Engineers' Handbook, McGraw-Hill, ISBN 0070498415, 2007.

[52] M. Peters, K. Timmerhaus, R. West, Plant Design and Economics for Chemical Engineers, McGraw-Hill Education, 2003.

[53] T. Lestina, R.W. Serth, Process Heat Transfer: Principles, Applications and Rules of Thumb, Elsevier Science, ISBN 9780080544410, 2010.

[54] C. Cooper, F. Kamakate, T. Reinhart, M. Kromer, R. Wilson, Reducing Heavy-Duty Long Haul Combination Truck Fuel Consumption and CO2 Emissions, NESCCAF, ICCT, SwRI, TIAX, LLC., 2009.

Table 1 Engine performance, input variables for heat recovery analysis and ORC modelling assumptions

HDDE performance			ORC assumptions		
Speed	rpm	1440	η_{exp}	%	65
$\dot{W}_{engine}$	kW	316	η_{pump}	%	55
η_{engine}	%	41.4	$\Delta P_{heat\ transfer}$	bar	0.2
			$T_{pp\ HEX}$	°C	25
ORC input variables			$T_{superheat}$	°C	5
T_{exh}	°C	420	$T_{pp\ IHE}$	°C	10
$c_{p\ exh}$	kJ/kg°C	1.15	$T_{condensing}$	°C	70
$\dot{m}_{exh}$	kg/s	0.4	$T_{subcooling}$	°C	5

Table 2 Key system, sizing and performance parameters for the conventional high-temperature fluids and their proposed blends

		Toluene	T80	MM	MM80
System parameters					
P_{max}	bar	9.1	23.8	7.9	17.9
P_{min}	bar	0.3	1.1	0.4	1
T_{max}	°C	216	243	193	207
T_{min}	°C	65	61	65	66
$T_{start\ of\ evaporation}$	°C	212	180	189	173
$T_{end\ of\ condensation}$	°C	70	66	70	71
$\Delta T_{evaporation\ (ideal)}$	°C	-	59	-	30
$\Delta T_{condensation\ (ideal)}$	°C	-	31	-	11
$\dot{m}_{fluid}$	kg/s	0.24	0.18	0.4	0.29
$\dot{V}_{pump}$	m^3/s	2.9e-4	2.2e-4	6.3e-4	4e-4
$\rho_{exp\ exit}$	kg/m^3	1.7	2.6	3.6	3.9
PR_{exp}		13.1:1	15.8:1	9.6:1	12.9:1
$\dot{Q}_{HEX}$	kW	110.2	111	113.3	112.1
$\dot{Q}_{IHE}$	kW	30.4	33.8	64.3	50.2
$\dot{Q}_{condenser}$	kW	95.4	93	100.7	96.5
$\dot{m}_{cooling\ air}$	kg/s	4.8	4.6	5	4.8
$\dot{W}_{exp}$	kW	15.2	18.9	13.4	16.8
$\dot{W}_{pump}$	kW	0.5	0.9	0.9	1.2
Size and design intensity parameters					
UA_{HEX}	W/°C	1560	1560	1390	1390
UA_{IHE}	W/°C	1775	1775	4015	4015
$UA_{condenser}$	W/°C	3320	3320	3820	3820
VFR_{exp}		14:1	14:1	12:1	12:1
Performance parameters					
$\eta_{I\ ORC}$	%	13.4	16.2	11.1	13.9
$\dot{W}_{net\ ORC}$	kW	14.8	18	12.6	15.6

748 Table 3 Blend screening methodology consisting of 22 screening criteria to achieve the innovative ORC approach

	Property	Toluene, MM	Blend constituent	Dual component blend
1	Latent heat of vaporisation (at 100°C)	368, 193 kJ/kg	≥ 1.25X	
2	Vapour density (at 100°C)	2.2, 5.5 kg/m^3	≥ 1.25X	
3	Condensation behaviour	Constant temperature		Temperature glide is a function of composition
4	Evaporation behaviour	Constant temperature		Temperature glide is a function of pressure
5	Toluene and MM mass concentration			≥ 66%
6	Available number of data sets			> 10 (error less than 2°C)
7	Market availability and industrial experience	Moderate to high	Moderate to high	
8	Fluid classification			Homogeneous positive pressure swing azeotrope
9	Thermal conductivity (at 100°C)	0.114, 0.106 W/m°C	≥ 1.25X	
10	Specific heat (at 100°C)	1.9, 2.07 kJ/kg°C	≥ 1.25X	
11	Boiling point	111, 101°C	≤ 100°C	
12	Number of atoms in a molecule	15, 27	6 to 15	
13	Freezing temperature	-95, -59°C	≤ -50°C	
14	Thermal decomposition temperature	> 308, > 300°C	≥ 250°C	
15	Auto-ignition	480, 340°C	≥ 350°C	
16	NFPA health rating	2, 1	≤ 2	
17	NFPA flammability rating	3, 3	≤ 3	
18	NFPA instability rating	0, 0	0	
19	ODP	< 0.00001	< 0.00001	
20	GWP	≈ 20	≤ 20	
21	Molecular makeup	C, H, O (and Si)	C, H, O (and Si)	
22	Compatibility		▪ Metals and alloys (aluminum, carbon steel, cast iron, copper, stainless steel) ▪ O-ring materials (ChemRaz, Kalrez) ▪ Thermoplastic (PTFE)	

749

750

751

752

753

754

755

756

757

758

759

760

761

762

763

764

765

766

Table 4 Key fluid properties for comparison between the blends and their pure fluid counterparts at the two possible extreme fluid conditions in an ORC

	Toluene	T80	MM	MM80
70°C Saturated liquid				
Molecular weight, M_{wt} g/mol	92	67	162	108
Pressure, $P_{saturation}$ bar	0.3	1.2	0.4	0.9
Density, ρ_{liquid} kg/m^3	822	831	712	735
Specific heat, c_p kJ/kg°C	1.77	2.29	1.96	2.27
Heat of vaporisation, H_{vap} kJ/kg	383	557	206	344
Thermal conductivity, λ_{liquid} W/m°C	0.121	0.129	0.115	0.121
Viscosity, $\mu_{dynamic}$ cP	0.352	0.341	0.3	0.381
170°C Saturated vapour				
Pressure, $P_{saturation}$ bar	4.1	7.1	5.3	9.7
Density, ρ_{vapour} kg/m^3	11.2	12.9	29.4	28.4
Specific heat, c_p kJ/kg°C	1.72	1.69	1.96	1.89
Heat of vaporisation, H_{vap} kJ/kg	324	527	151	311
Thermal conductivity, λ_{vapour} W/m°C	0.025	0.027	0.023	0.026
Viscosity, $\mu_{dynamic}$ cP	0.01	0.012	0.011	0.011

Table 5 Equations representing the conceptual equipment cost estimates that were adjusted to the findings of the original cost analysis study

Equipment	Technology	Dependent variable	Purchase cost ($)	Material	Range of application
Working fluid pump (primary option)	Reciprocating pump including motor	Discharge volumetric flowrate ($V_{pump\ exit}$, m^3/s) and discharge pressure ($P_{pump\ exit}$, kPa)	$(1544 + 0.237\ P)^* (0.633 + 667\ V)$	Carbon Steel	0.0001 to 0.001 m^3/s 1035 to 5000 kPa
Working fluid pump (secondary option)	Gear pump including gear transmission	Discharge volumetric flowrate ($V_{pump\ exit}$, m^3/s)	$6348\ V^{0.25}$	Cast iron case, iron alloy gears, steel shaft	0.0001 to 0.001 m^3/s Pressure ≤ 4140 kPa
Condenser	Air cooled condenser including fan and motor	Area (A_{cond}, m^2) and balance of the engine cooling module	$3788\ A^{0.42}$	Carbon Steel	Pressure ≤ 1035 kPa Area ≤ 500 m^2 (area equivalent to bare tubes excluding fins)
IHE (primary option)	Welded plate heat exchanger	Area (A_{IHE}, m^2)	$1926 + 28\ A$	Carbon Steel	Pressure ≤ 1035 kPa Area ≤ 500 m^2
IHE (secondary option)	Gasketed plate heat exchanger	Area (A_{IHE}, m^2)	$603 + 12.2\ A$	Carbon Steel	Pressure ≤ 3000 kPa Area ≤ 500 m^2
HEX (primary option)	Shell and fixed-tube heat exchangers (evaporator type for direct exhaust heat)	Area (A_{HEX}, m^2) and pressure ($P_{HEX\ inlet}$, kPa)	$(2601 + 121\ A - 0.25\ A^2)^* (0.00002\ P + 0.95)$	Carbon steel shell and tube	Shell ≤ 1035 kPa Tube ≤ 5000 kPa Area ≤ 100 m^2
HEX (secondary option)	Shell and plate heat exchanger (evaporator type for direct exhaust heat)	Area (A_{HEX}, m^2)	$113 + 113\ A$	Carbon steel shell and plate	Pressure ≤ 4140 kPa Area ≤ 100 m^2
Expansion machine	Radial turbine (gas and liquid type) including generator	Recovered power (W_{exp}, kW)	$12664 + 197\ W$	Carbon Steel	10 to 100 kW
Pipe	Welded and screwed	Diameter (D_{pipe}, m) and length (L_{pipe}, m)	$82\ L^* (24\ D + 0.08)$	Carbon Steel	Diameter = 0.015 to 0.06 m Length = 1 to 100 m
Storage tank	Horizontal with round ends	Volume (V_{tank}, L)	$40\ V^{0.58}$	Carbon Steel	10 to 400 L
Expansion machine bypass valve	Pressure Reducing Valve (PRV)	Diameter (D_{PRV}, m)	$103 + 15035\ D$	Carbon Steel	0.01 to 0.1 m

Table 6 Absolute and specific costs for the primary and secondary ORC options utilising the blends and their pure fluid counterparts

	Fluid	Pipe	Tank	PRV	Controls and instrumentation	Additional hardware	Pump	IHE	HEX	Condenser	Turbine-generator	Total cost ($)	Cost per net power ($/kW)
Primary options													
Toluene	153	271	288	329	900	900	1454	2175	5191	8577	15658	35895	2434
T80	324	271	288	329	900	900	1644	2175	5348	8577	16387	37142	2061
MM	225	271	288	329	900	900	1832	2489	4902	9072	15324	36530	2906
MM80	204	271	288	329	900	900	1771	2489	5004	9072	15974	37200	2392
Secondary option													
Toluene	153	271	288	329	900	900	828	712	2825	8577	15658	31440	2132
T80	324	271	288	329	900	900	773	712	2825	8577	16387	32285	1792
MM	225	271	288	329	900	900	1006	848	2531	9072	15324	31692	2521
MM80	204	271	288	329	900	900	898	848	2531	9072	15974	32214	2072

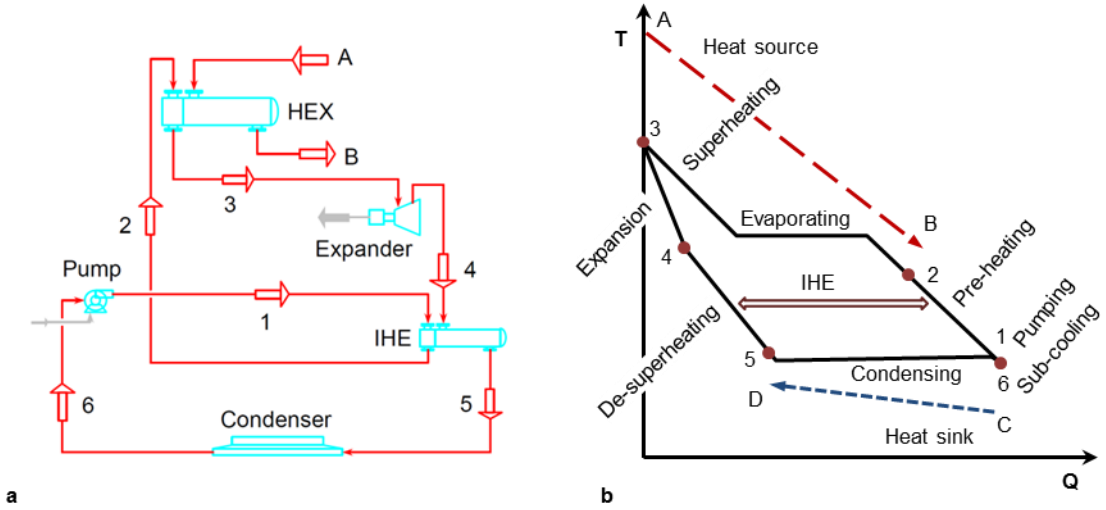

Figure 1 Considered ORC with an IHE (a) Simplified system schematic, and (b) T-Q sketch under superheated subcritical operation

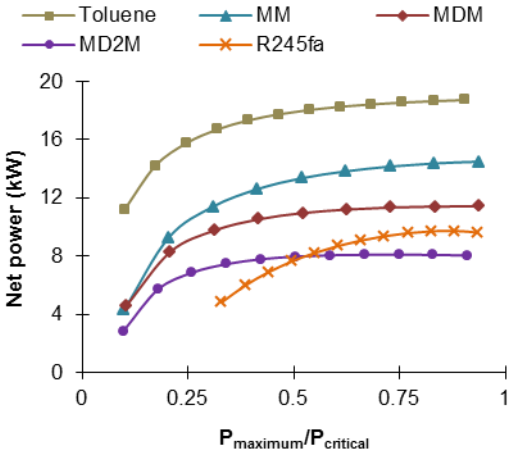

Figure 2 Net power comparison for the commonly suggested high-temperature fluids and R245fa on the bases of a non-constrained expansion machine size

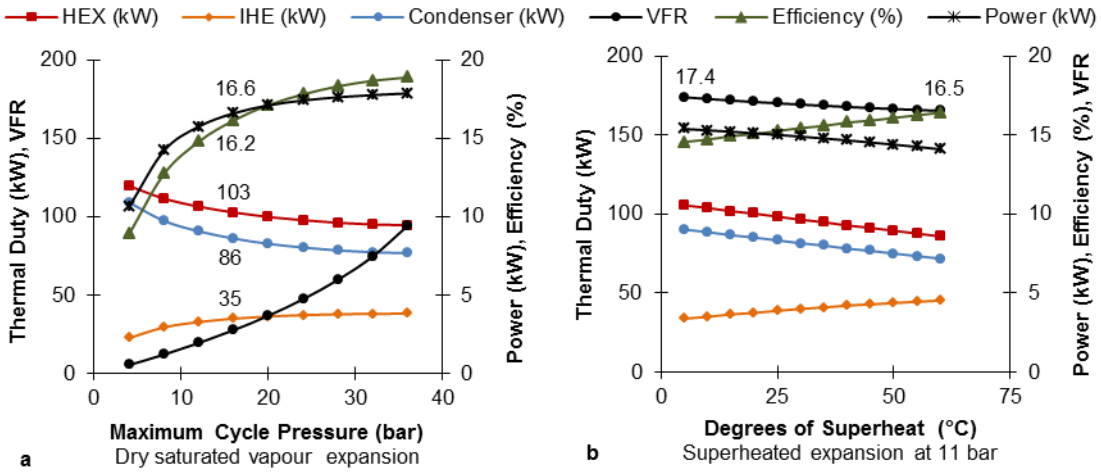

Figure 3 Effect on thermal duty and performance for toluene cycle by (a) Variation in cycle pressure, and (b) Variation in cycle superheat

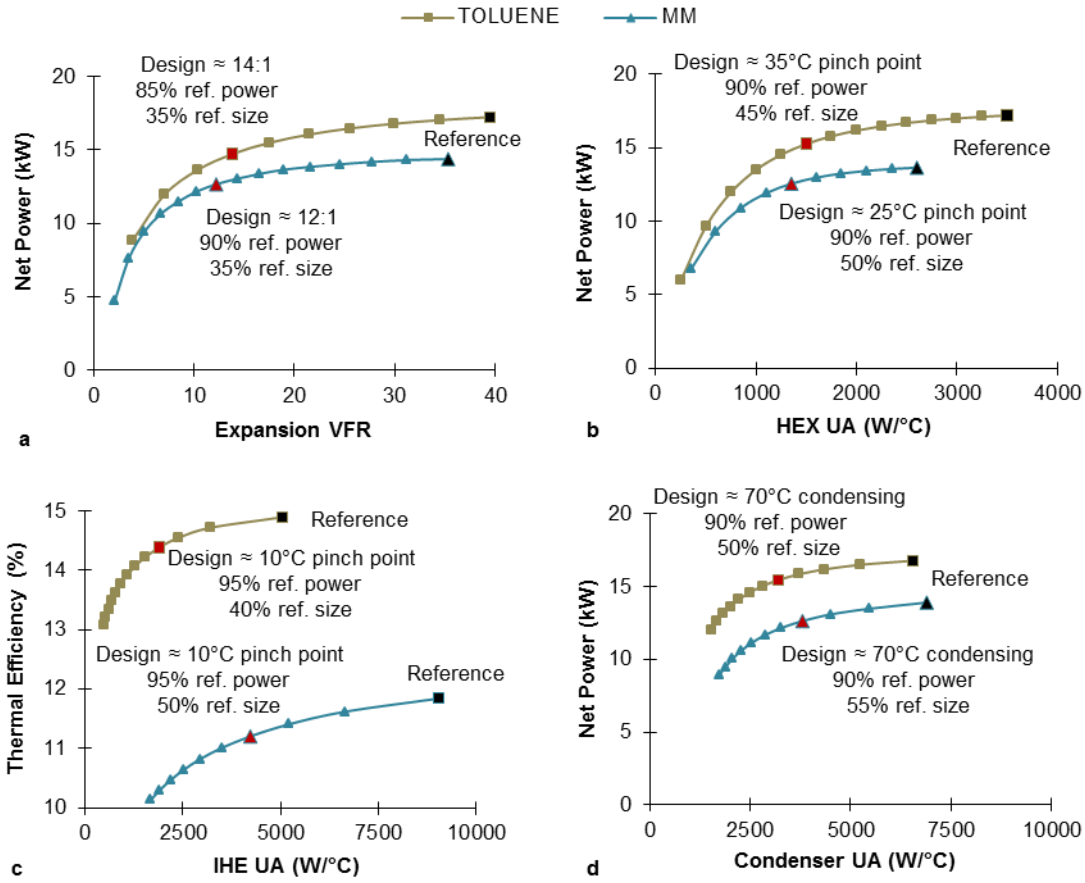

Figure 4 Equipment size and system performance trade-off for (a) Expansion machine, (b) Exhaust heat exchanger, (c) Internal heat exchanger, and (d) Air condenser

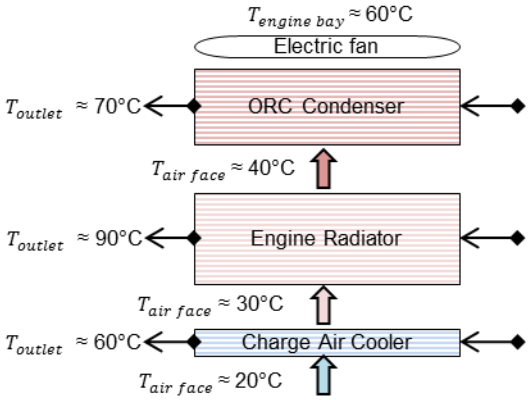

Figure 5 Schematic of the modified engine cooling module with an additional high-temperature condenser, showing radiator/condenser outlet temperature as a function of air temperature rise through the module

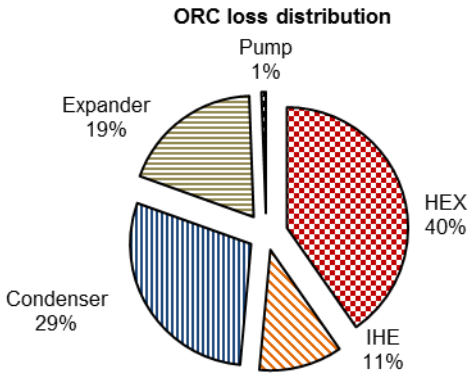

Figure 6 Irreversibility contributions by the toluene ORC processes at the design point condition

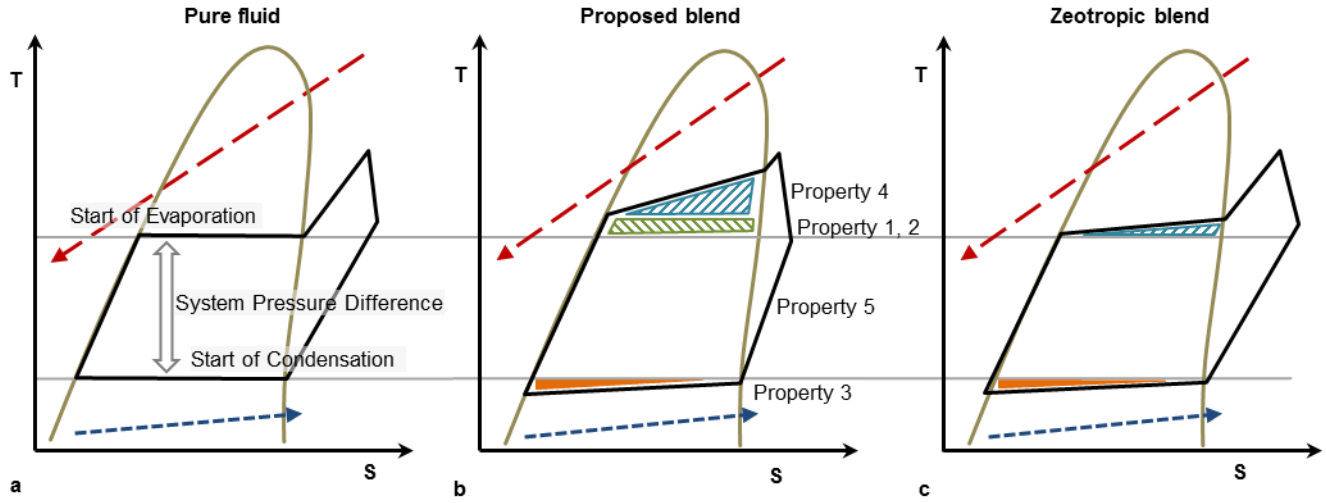

Figure 7 Comparing conceptual T-S diagrams and areas of loss reduction (a) Conventional ORC, (b) Proposed ORC, and (c) Conventional zeotropic ORC

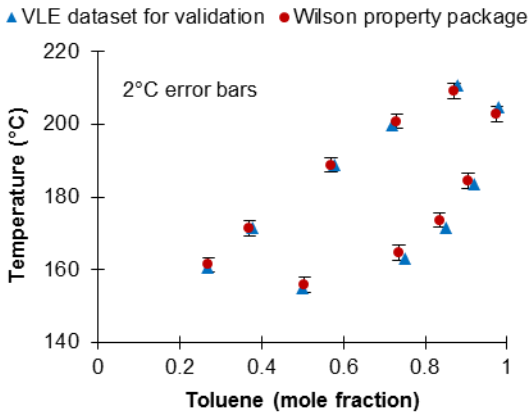

Figure 8 Validation of the VLE behaviour for the chosen fluid property package

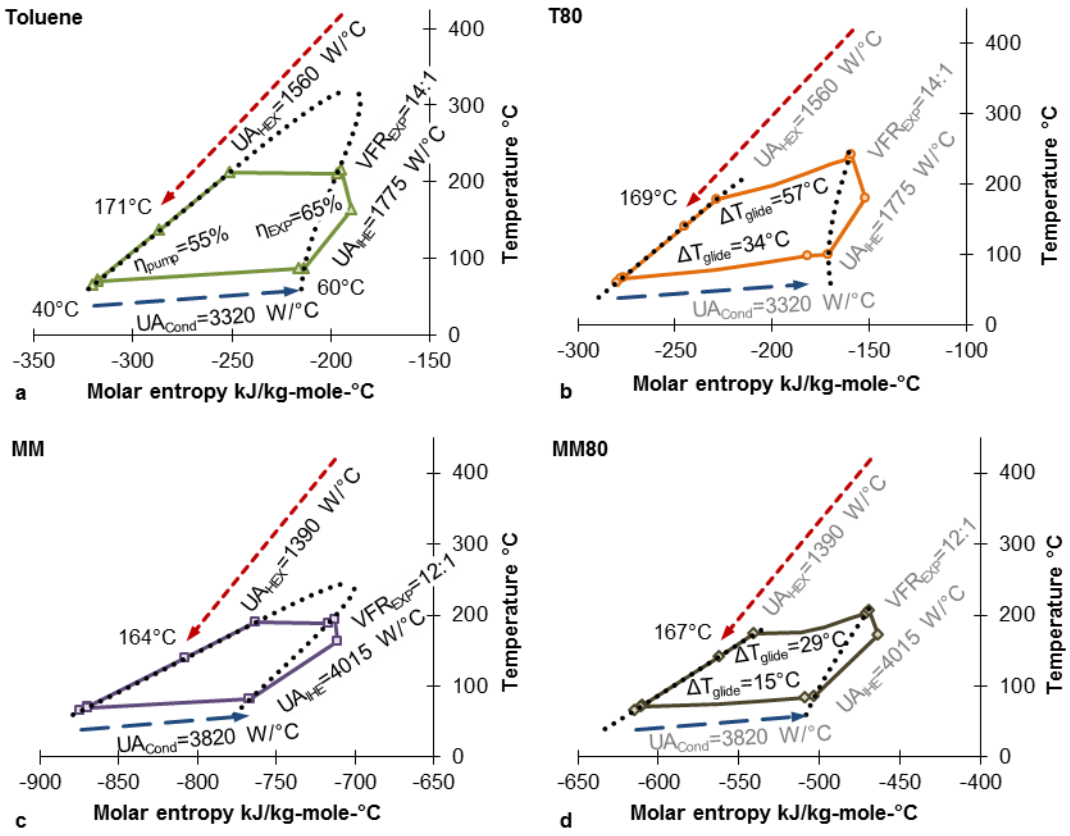

Figure 9 Comparing T-S diagrams under equivalent size and design intensity (a,b) Design point toluene vs. proposed T80, and (c,d) Design point MM vs. proposed MM80

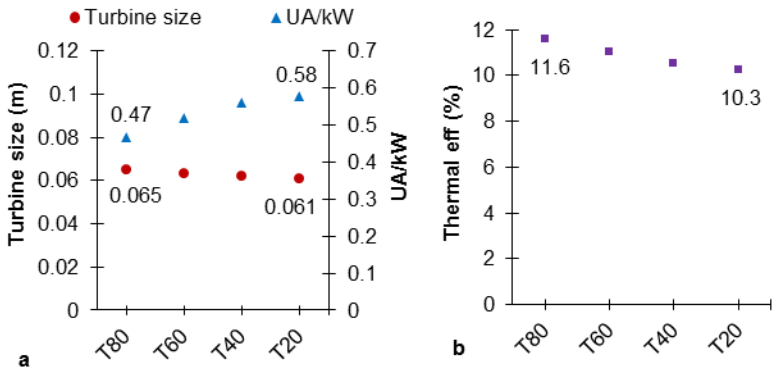

Figure 10 Effect of varied toluene concentration on (a) Turbine size parameter and normalised heat transfer footprint, and (b) Thermal efficiency

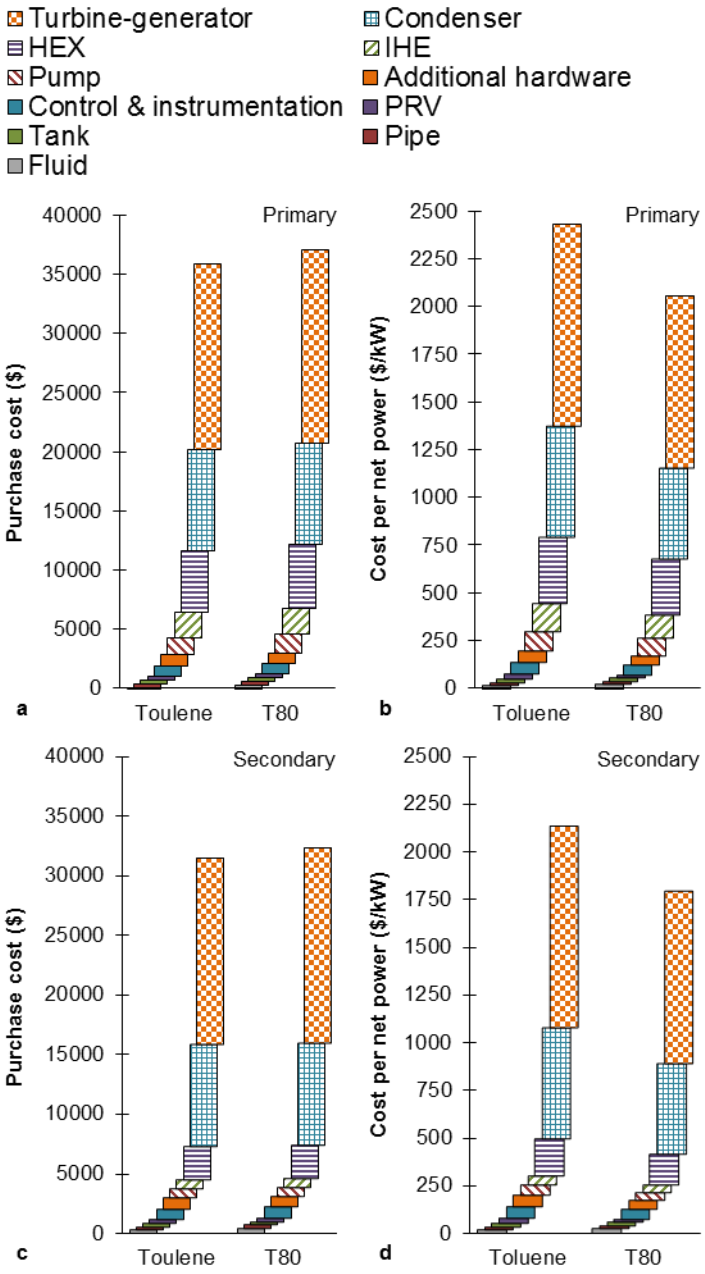

Figure 11 Comparison between toluene and T80 (a) Absolute costs for the primary option, (b) Specific costs for the primary option, (c) Absolute costs for the secondary option, and (d) Specific costs for the secondary option